# Multimodal Active Measurement for Human Mesh Recovery in Close Proximity

Takahiro Maeda<sup>1\*</sup>, Keisuke Takeshita<sup>2</sup>, Norimichi Ukita<sup>1</sup>, and Kazuhito Tanaka<sup>2</sup>

Abstract—For physical human-robot interactions (pHRI), a robot needs to estimate the accurate body pose of a target person. However, in these pHRI scenarios, the robot cannot fully observe the target person's body with equipped cameras because the target person must be close to the robot for physical interaction. This close distance leads to severe truncation and occlusions and thus results in poor accuracy of human pose estimation. For better accuracy in this challenging environment, we propose an active measurement and sensor fusion framework of the equipped cameras with touch and ranging sensors such as 2D LiDAR. Touch and ranging sensor measurements are sparse but reliable and informative cues for localizing human body parts. In our active measurement process, camera viewpoints and sensor placements are dynamically optimized to measure body parts with higher estimation uncertainty, which is closely related to truncation or occlusion. In our sensor fusion process, assuming that the measurements of touch and ranging sensors are more reliable than the camera-based estimations, we fuse the sensor measurements to the camera-based estimated pose by aligning the estimated pose towards the measured points. Our proposed method outperformed previous methods on the standard occlusion benchmark with simulated active measurement. Furthermore, our method reliably estimated human poses using a real robot, even with practical constraints such as occlusion by blankets.

#### I. INTRODUCTION

3D human pose estimation is crucial for assistive robots to physically interact with humans. For example, to achieve care robots help elderly or physically challenged people stand up stably, robots need the information of the human body to detect unstable postures and falling to decide where to support with their arms. However, in these physical human-robot interactions (pHRI) scenarios, robots usually cannot fully observe the human body with equipped cameras because occlusions and image truncations happen at a very close range. Human pose estimation methods perform poorly with these settings due to limited information, as shown in the upper part of Fig. 1.

However, humans can still estimate another person's pose in very close range by actively moving their heads and eyes to a more informative viewpoint and using multimodal cues such as tactile information. Physically interactive robots should perform the same by actively operating their joints and wheels/legs and fuzing multimodal sensor inputs, as shown in the bottom part of Fig. 1.

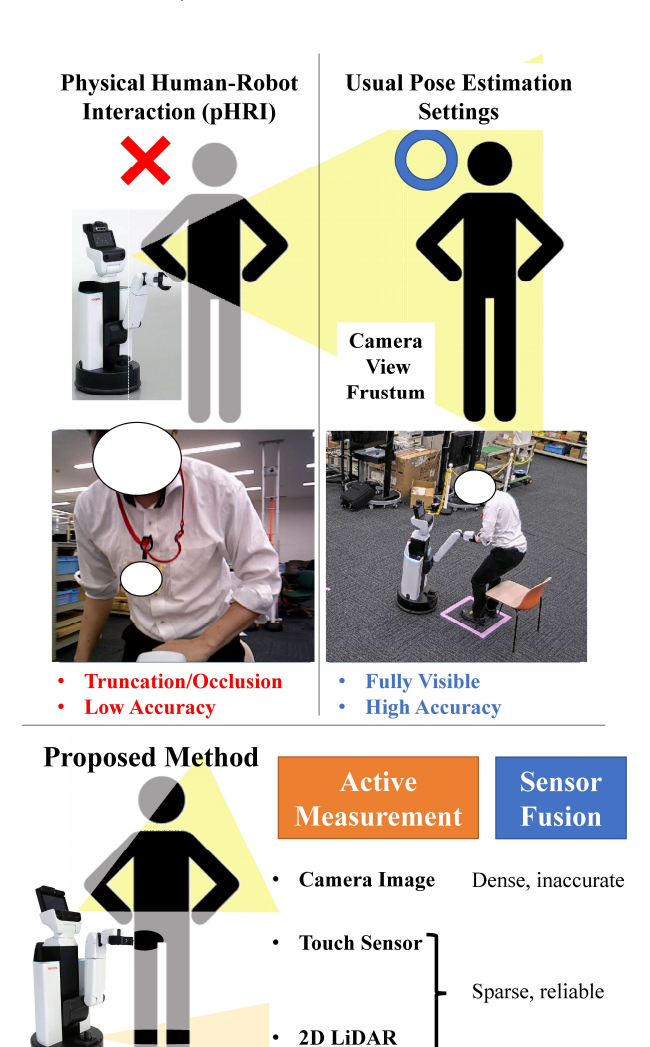


Fig. 1: Problem of previous human pose estimation methods in pHRI scenarios and our proposed method.

To achieve this, we propose a new human pose estimation method for physically interactive robots. Our proposed method has two components: *active measurement* and *sensor fusion*. In the *active measurement*, the camera viewpoints and sensor placements are dynamically optimized to reduce the unobserved body parts by truncations and occlusions. In the *sensor fusion*, estimated poses from cameras are improved by aligning the body poses consistent with sensor measurements. Specifically, we minimize the distance between the estimated body surface and the sensor measurement points. Our contributions are as follows:

<sup>\*</sup>Work done during the internship at Frontier Research Center, Toyota Motor Corporation sd21601@toyota-ti.ac.jp

<sup>&</sup>lt;sup>1</sup>Toyota Technological Institute, Nagoya, Aichi, Japan.

<sup>&</sup>lt;sup>2</sup>R-Frontier Division, Frontier Research Center, Toyota Motor Corporation, Toyota, Aichi, Japan.

- We propose the active measurement framework for human pose estimation using multimodal sensors. This framework maximizes the observation area of sensors to cover the whole body.
- Our sensor fusion method improves the estimated human pose from optical images by reconfiguring them to coincide with measurements of the human body surface measured from the multimodal sensors.
- Our proposed method outperforms previous methods on the standard occlusion benchmark with simulated active measurement. We further demonstrate the accuracy improvement of our proposed method with real-world experiments using a robot in application scenarios.

#### II. RELATED WORK

There has been significant progress in human pose estimation from RGB images, starting from 2D [5], [35] to 3D [24], [33], [42] and mesh recovery [4], [15], [40]. However, most existing methods assume input images are taken from enough distance without occlusions and view-dependent truncations. Therefore, the following three techniques should be considered in physical human-robot interaction scenarios to deal with occlusions and truncations in close proximity.

Image-based Pose estimation robust to occlusions and view-dependent truncations. Some methods utilize attention mechanisms to focus on visible body parts to ensure the robustness to occlusions [11], [17], [20]. However, it is difficult to adequately train attention mechanisms due to the scarcity of occluded data. Data augmentation [28], [37] is an easy way for simulating these occluded or truncated data. Still, it cannot fully capture the complexity of real-world occlusions and truncations. Some methods use probabilistic models to regress multiple pose hypotheses [3], [13], [21] for ill-posed problems, such as human pose estimation on severely truncated and occluded images.

Although these methods above can improve estimated poses on ambiguous images, their estimations are just guessing truncated or occluded body parts. Robots can move to viewpoints with fewer occlusions and truncations in physical human-robot interaction scenarios.

Pose estimation with active measurements. The quality of viewpoints is often expressed as estimated error metrics or uncertainty of human pose estimation [6], [18]. Specifically, Kiciroglu *et al.* [18] performs quadratic approximation to error landscape on each viewpoint and treats the approximated variance as uncertainty. However, this method assumes no truncations and thus fails to model the complex error landscape with severe truncations. On the other hand, Arzati *et al.* [2] optimizes flight drone viewpoints by deep reinforcement learning for dermatology applications. DQN [25] is trained in simulation environments based on the reward related to pose estimation accuracy. However, this reward considers only visible body parts and ignores the view-dependent truncated body parts.

Although camera active measurements above can estimate the best camera viewpoint, robots usually have multimodal sensors other than cameras. Multimodality may improve pose estimation accuracy by complementing limited information from camera observations. Our proposed active measurement can dynamically optimize camera viewpoints, touch, and ranging sensor positions.

Pose estimation with multimodal data. Wearable Inertia Measurement Units (IMUs) attached to human body parts can track their positions and orientations and thus help human pose estimation [12], [32]. However, it is inconvenient to wear IMUs for robots' assistance. Furthermore, wearing IMUs for a long time causes drifting and results in less accurate measurements.

RGB-D cameras and 3D point cloud sensors are often utilized other than RGB cameras [14], [34], [36]. Although these sensors can alleviate depth ambiguity and provide accurate estimations, they have a minimum depth distance of around 50 centimeters for measurements, which is inappropriate for human pose estimation in close range.

The sensors above are difficult to utilize in pHRI settings due to the amount of effort required to wear IMUs and the minimum depth distances of depth sensors. Therefore, we focus on the cues obtained during pHRI, such as touch sensors and 2D LiDARs, which have a minimum distance of around one centimeter, unlike 3D point cloud sensors. Touch and 2d ranging sensors are sparse compared to 3D point cloud sensors, but reliable cues in pHRI scenarios. The other possible options are discussed in Sec. VI.

#### III. PRELIMINARY

# A. SMPL Model

We represent human poses using Skinned Multi-person Linear Body (SMPL [23]). SMPL is a neural network representation  $\mathcal{M}(\theta,\beta) = V_{\text{local}}$  that maps a set of pose parameters  $\theta$  and body parameters  $\beta$  to a human body mesh in the pelvis-centered local coordinates  $V_{\text{local}} \in \mathbb{R}^{3 \times 6890}$  with 6890 vertices. The pose parameters  $\theta$  contain each body joint rotation. The shape parameters  $\beta$  control the body height, weights, and limb length. We can obtain the human body mesh on the world coordinates V using a global pose as  $V = R_p V_{\text{local}} + t_p$ , where the global pose is a set of global translation and rotation of the pose  $(R_p, t_p)$ . Global body joint positions J are also regressed by a linear regressor W as  $J = R_p W V_{\text{local}} + t_p$ . We use the mesh vertices V to fuse the touch and ranging sensor measurements into the estimated pose, as explained in Sec. IV-D.

# B. Probabilistic Human Mesh Recovery

Human mesh recovery is a task to estimate the set of pose parameters  $\boldsymbol{\theta}$ , body parameters  $\boldsymbol{\beta}$ , and global pose  $(R_p, t_p)$ , which defines human mesh vertices V and eventual joint positions J in the world coordinates, given the camera image I containing a person. Image-conditioned probability distribution  $p(\boldsymbol{\theta}, \boldsymbol{\beta}|I)$  is obtained by the probabilistic human mesh recovery. Given this distribution, we can also regress

the pose via maximum likelihood as follows.

$$V_{\rm ML} = R_p \mathcal{M}(\boldsymbol{\theta}_{\rm ML}, \boldsymbol{\beta}_{\rm ML}) + \boldsymbol{t}_p \tag{1}$$

$$J_{\rm ML} = R_p W \mathcal{M}(\boldsymbol{\theta}_{\rm ML}, \boldsymbol{\beta}_{\rm ML}) + \boldsymbol{t}_p \tag{2}$$

where, 
$$\theta_{\text{ML}}, \beta_{\text{ML}} = \underset{\theta, \beta}{\operatorname{arg max}} p(\theta, \beta | I)$$
 (3)

# IV. PROPOSED METHOD

The overview of our proposed method is shown in Fig. 2. Our proposed method is robot-agnostic.

#### A. Notation

The objective is to estimate human 3D joint positions  $J \in \mathbb{R}^{3 \times N_{\mathrm{joint}}}$ , where  $N_{\mathrm{joint}}$  is the number of joints. The available information is multimodal measurements including a camera image  $I(R_c, \boldsymbol{t}_c)$  and touch and ranging K sensor placements  $(R_1, \boldsymbol{t}_1), \ldots, (R_K, \boldsymbol{t}_K)$  such as 2D LiDAR and a touch sensor measuring the person's body surface, where  $R_c$  and  $\boldsymbol{t}_c$  are the camera orientation and translation, and  $R_k$  and  $\boldsymbol{t}_k$  are the k-th sensor orientation and translation accordingly.

#### B. Uncertainty Estimation

We use a probabilistic approach [21] to utilize the estimation uncertainty  $\sigma^{mesh}$  in our active measurement. The uncertainty of the estimated pose is calculated as positional variances  $\sigma^{mesh} \in \mathbb{R}^{6890}$  of each mesh vertex as follows,

$$\sigma^{\text{mesh}} = \mathbb{E}_{p(\boldsymbol{\theta}, \boldsymbol{\beta}|I)}[(\mathcal{M}(\boldsymbol{\theta}, \boldsymbol{\beta}) - \bar{\mathcal{M}}(\boldsymbol{\theta}, \boldsymbol{\beta})^2]$$
 (4)

$$\bar{\mathcal{M}}(\boldsymbol{\theta}, \boldsymbol{\beta}) = \mathbb{E}_{p(\boldsymbol{\theta}, \boldsymbol{\beta}|I)}[\mathcal{M}(\boldsymbol{\theta}, \boldsymbol{\beta})] \tag{5}$$

, where  $\mathbb{E}_{p(\theta, \beta|I)}$  denotes the expectation over the pose distribution conditioned by a image. There are many examples that utilize predictive variances as uncertainty. One example is a large family of Bayesian Neural Networks [10], [16]. They estimate the aleatoric uncertainty of trained models as predictive variances. This uncertainty of estimated pose  $\sigma^{ ext{mesh}}$  can account for the occluded or truncated body parts by learning possible pose distributions of observed occluded human images, as shown in Fig. 2. Sengupta et al. [29] showed the per-vertex uncertainty closely correlated to the occluded and truncated body parts. We chose implicit uncertainty estimation as predictive variances for two reasons. First, predictive variances account for body kinematics using the joint model. For example, the camera-truncated lower leg position is stably predicted if its knee joint is visible. Thus, the uncertainty of the lower leg is low using predictive variances, whereas one can be wrongly high using just explicit camera information. Second, camera view information still needs object detection to estimate the uncertainty from occlusion, whereas predictive variances do not. We can determine the effective camera and sensor positions based on the estimated uncertainty  $\sigma^{\text{mesh}}$  via our active measurement framework.

#### C. Active Measurement

The camera viewpoint and sensor placements  $(R_c, \boldsymbol{t}_c), (R_1, \boldsymbol{t}_1), \dots, (R_K, \boldsymbol{t}_K)$  are optimized based on the uncertainty of the estimated pose  $\boldsymbol{\sigma}^{\text{mesh}}$ . We optimize each placement one by one. Specifically, after optimizing

one sensor, we update the estimated pose and uncertainty  $\sigma^{\text{mesh}}$  based on the sensor fusion as described in Sec. IV-D. We first optimize the camera viewpoint since images usually have the richest information about poses.

Camera viewpoint optimization: It is difficult to directly optimize camera viewpoints to maximize pose estimation accuracy. Therefore, we propose to maximize the information obtained from cameras. Specifically, Camera viewpoint  $(R_c, t_c)$  is optimized to cover the largest body surface within the camera image and reduce truncation and self-occlusion. We use weighted coverage with the estimated uncertainty  $\sigma^{\text{mesh}}$  to cover possibly more erroneous body parts, which are considered to have higher uncertainty. Camera viewpoints are evaluated based on weighted mesh coverage as follows:

$$R_c^*, \boldsymbol{t}_c^* = \operatorname*{arg\,max}_{R_c, \boldsymbol{t}_c} \sum_{\boldsymbol{v}_i \in V_{\text{ML}}} \sigma_i^{\text{mesh}} f_i^{\text{visible}}$$
(6)

where,  $f_i^{\text{visible}}$  is the boolean for visibility of the 3D position of *i*-th vertex  $v_i$  from the mesh vertices V.  $f_i^{\text{visible}}$  is calculated by the camera projection function  $\pi$  that projects a 3D position to the 2D image coordinates and checks self-occlusion as follows:

$$f_i^{\text{visible}} = \begin{cases} 1 & \text{if } 0 \le x_i \le W, 0 \le y_i \le H, \text{Occ}_i = 0\\ 0 & \text{otherwise} \end{cases}$$
 (7)

$$x_i, y_i, Occ_i = \pi(\boldsymbol{v}_i; V, R_c, \boldsymbol{t}_c),$$
 (8)

where  $x_i, y_i$  are projected positions on the 2D image coordinates. W, H are the width and height of the input camera image.  $Occ_i$  denotes the boolean for self-occlusion as  $Occ_i \in \{0,1\}$  calculated based on the Z-buffer method. Specifically, we calculate the distances to all faces on each camera ray to determine whether faces are visible.  $Occ_i$  on each point is 0 if the point is contained by visible faces or 1 if contained by occluded faces. Although Eq. (6) can evaluate camera viewpoints, this is not differentiable and unsuitable for backpropagation. Therefore, the camera viewpoint is optimized by picking the best from a predefined set of viewpoints. The method is explained with one camera for brevity, but one can easily extend the viewpoint optimization to multiple cameras.

Touch and ranging sensor placement optimization: For touch and ranging sensors that measure the body surface, its placements  $(R_1, t_1), \ldots, (R_K, t_K)$  are optimized to complement the limited information from the optimized viewpoint. Specifically, we optimize the placements to measure the most uncertain vertex within kinematically possible placements by solving inverse kinematics (IK) as follows:

$$q_i, \operatorname{Suc}_i = \operatorname{IK}(\boldsymbol{v}_i; (R_c^*, \boldsymbol{t}_c^*), (R_1^*, \boldsymbol{t}_1^*), \dots, (R_{k-1}^*, \boldsymbol{t}_{k-1}^*))$$
 (9)

$$i^* = \underset{i \in [1,6890]}{\arg \max} \sigma_i^{\text{mesh}} \operatorname{Suc}_i$$
(10)

$$R_k^*, \boldsymbol{t}_k^* = FK(q_{i^*}) \tag{11}$$

where IK is the inverse kinematics function that takes a 3D position  $v_i$  of *i*-th mesh vertex and already optimized sensor placements  $(R_c^*, t_c^*), (R_1^*, t_1^*), \ldots, (R_{k-1}^*, t_{k-1}^*)$  as input, and outputs the joint parameters  $q_i$  which sensing the

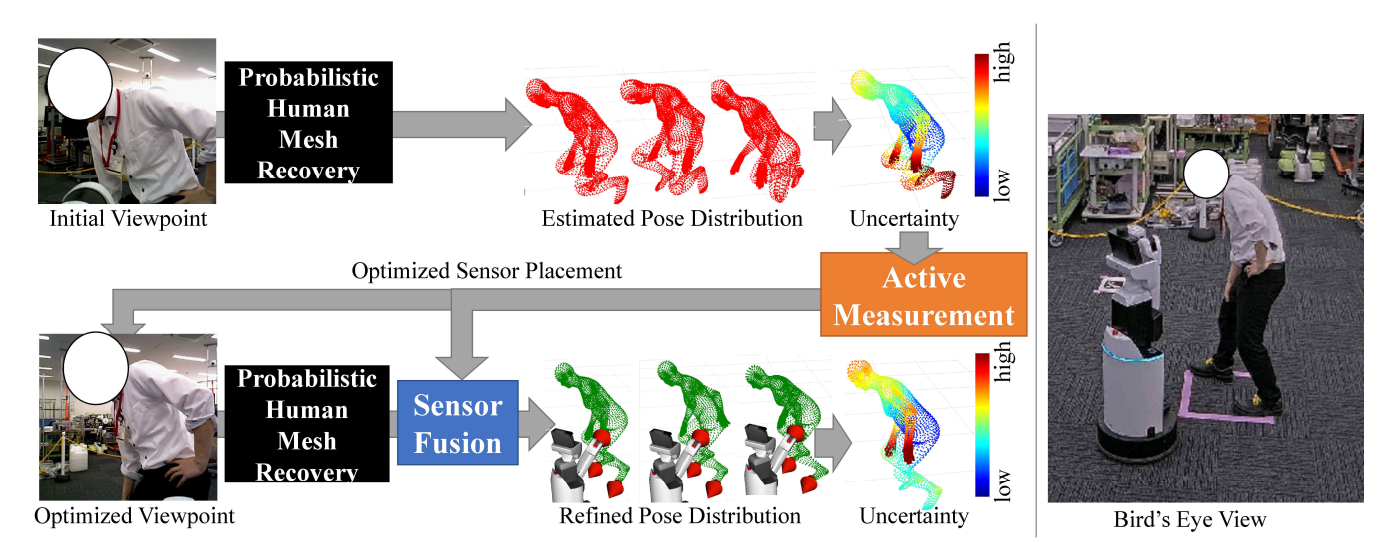


Fig. 2: Overview of our proposed method.

3D position  $v_i$  of *i*-th mesh vertex with the target sensor and  $\operatorname{Suc}_i \in 0, 1$  denotes the boolean for whether there is feasible joint parameters  $q_i$  satisfying the all optimized sensor placements. FK is the forward kinematics function that calculates the target sensor position  $R_k, t_k$  from the joint parameters q. After this optimization, we fuse the multimodal cues to the estimated pose.

#### D. Sensor Fusion

Our sensor fusion improves estimated poses by aligning the estimated mesh V consistent with the depth measurements of human body surface from currently optimized k sensors  $m_1, \ldots, m_k$ . The proposed sensor fusion has two stages: global position offset and local pose optimization.

**Global position offset:** We offset the global position  $t_p$  because camera-based estimated poses contain depth ambiguity due to an unknown person's height and inaccurate camera intrinsics. The offset is the mean vector between the measurements  $m_1, \ldots, m_k$  to the nearest mesh vertex  $w_1, \ldots, w_k$  from  $V_{\text{ML}}$  as follows:

$$\boldsymbol{t}_{\text{offset}} = \mathbb{E}_{(\boldsymbol{\theta}, \boldsymbol{\beta}) \sim p(\boldsymbol{\theta}, \boldsymbol{\beta}|I)} \left[ \frac{1}{k} \sum_{k'=1}^{k} \boldsymbol{w}_{k'} - \boldsymbol{m}_{k'} \right]$$
 (12)

$$\boldsymbol{w}_k = \operatorname*{arg\,min}_{\boldsymbol{v}_i} ||\boldsymbol{v}_i - \boldsymbol{m}_k|| \tag{13}$$

**Local pose optimization:** After calculating offset, we optimize each sampled pose parameter  $\theta$  by minimizing the distance between the body surface and the sensor measurements via backpropagation as follows:

$$\boldsymbol{\theta}^* = \operatorname*{arg\,min}_{\boldsymbol{\theta}} L \tag{14}$$

$$L = -p(\boldsymbol{\theta}, \boldsymbol{\beta}|I) + \frac{\alpha}{k} \sum_{k'=1}^{k} \boldsymbol{w}_{k'} - \boldsymbol{m}_{k'} - \boldsymbol{t}_{\text{offset}}$$
 (15)

where  $\alpha$  is a weighting parameter set as 0.01. Using each optimized pose parameter  $\theta^*$ , we update the positional variance  $\sigma^{\text{mesh}}$  as described in Sec. IV-B and optimize the next sensor

placement  $R_{k+1}$ ,  $t_{k+1}$  by repeating the process iteratively. The updated positional variance  $\sigma^{\text{mesh}}$  is expected to be small around the sensor measurements thanks to optimization. Therefore, the next measured point is a different uncertain vertex based on  $\sigma^{\text{mesh}}$ . The maximum-likelihood pose with sensor fusion  $\theta_{\text{ML}}^*$  is used for evaluation.

# V. EXPERIMENTS

We benchmarked the proposed method on the pose estimation dataset with occlusion by simulated active measurements in Sec. V-A. For real-world experiments, settings are described in Sec. V-B. We report the quantitative results of the real-world experiments in Sec. V-C. The qualitative results under more constraints are described in Sec. V-D.<sup>1</sup>

#### A. Quantitative Comparison on Benchmark

We compare the proposed and previous methods on 3DPW-OC [31], [43], the standard benchmark for human pose estimation with occlusion. 3DPW-OC contains pairs of images and ground truth SMPL mesh annotations. We omitted the camera viewpoint optimization because we cannot optimize and retake the input images in the benchmark dataset. For touch and ranging sensors, we simulated the measured vertices by sampling from ground truth mesh and adding a artificial Gaussian noise  $\sigma=0.02 [\rm m]$ . The  $\sigma$  value is determined based on the 95 percent confidence interval  $2\sigma=0.04 [\rm m]$  of the range sensor accuracy within  $\pm 0.04 [\rm m]$  and HSR's hand accuracy within  $\pm 0.02 [\rm m]$ .

The second column of the Tab. I denotes the number of measured vertices. We used ProHMR [21] as the off-the-shelf probabilistic human mesh recovery. However, model weights were trained from scratch with a focal length of 2200 to deal with the changing focal length of input images [19]. To validate the proposed active measurement and sensor fusion separately, we compare these with naive measurements and

<sup>1</sup>The code is publicly available at https://github.com/meaten/ HMRinCloseProximity.

TABLE I: Quantitative results on 3DPW-OC in [mm]. RM and AM denote random measurement and our active measurement. CS and SF denote the closest sample selection and our sensor fusion.

Method	Measured Vertices	MPJPE↓	PA-MPJPE↓
I2L-MeshNet [26]	n=0	92.0	61.4
SPIN [12]	n=0	95.5	60.7
PyMAF [41]	n=0	89.6	59.1
ROMP [30]	n=0	91.0	62.0
OCHMR [17]	n=0	112.2	75.2
PARE [20]	n=0	83.5	57.0
3DCrowdNet [7]	n=0	83.5	57.1
JOTR [22]	n=0	75.7	52.2
ProHMR [21]	n=0	92.9	62.2
	n=3	89.0	62.3
ProHMR + RM + CS	n=5	87.1	60.7
	n=10	84.9	58.8
	n=30	82.7	57.1
ProHMR + RM + SF	n=3	86.0	61.6
	n=5	81.6	58.4
	n=10	75.6	53.7
	n=0         92.0           n=0         95.5           n=0         89.6           n=0         91.0           n=0         112.2           n=0         83.5           n=0         75.7           n=0         92.9           n=3         89.0           n=5         87.1           n=10         84.9           n=30         82.7           n=3         86.0           n=5         81.6           n=10         75.6           n=30         68.5           n=3         88.3           n=5         86.3           n=10         84.1           n=30         82.7           n=3         83.5           n=5         78.0           n=10         71.1	47.6	
	n=3	88.3	61.1
ProHMR + AM + CS	n=5	86.3	59.5
	n=10	84.1	57.9
	n=30	82.7	57.2
	n=3	83.5	59.2
ProHMR + AM + SF	n=5	78.0	55.1
Prohmk + AM + SF	n=10	71.1	49.3
	n=30	67.2	46.1

fusion methods. Therefore, we replace the proposed method with random measurement (RM) and closest sample selection (CS). RM randomly measures the mesh points, unlike our active measurement (AM) choosing the most uncertain mesh points. CS selects the pose closest to the measurements within samples from the pose distribution  $p(\theta, \beta|I)$ , unlike our sensor fusion (SF) aligning the closest pose via optimization. We report the mean per joint position error (MPJPE) in Tab. I. The results show the methods with our sensor fusion significantly increase the accuracy with sparse but reliable sensor measurements. Our active measurement can further improve the accuracy of our sensor fusion. The computational costs of our active measurement and sensor fusion are  $6.4 \pm 2.0 [\text{ms}]$  and  $2417.7 \pm 814.4 [\text{ms}]$  with Intel Xeon Gold CPU and one NVIDIA RTX TITAN GPU.

#### B. Experimental Setup of Real-World Experiments

Toyota Human Support Robot (HSR) [38], [39], shown in the bottom of Fig. 1, was used in the real-world experiments. The HSR has RGB cameras, a force sensor in the wrist joint, and 2D LiDAR. The RGB camera has 5 degrees of freedom by the omnidirectional moving base, the lifting joint, and the pan/tilt joint. The force sensor has 3 degrees of freedom by the yaw rotation of the omnidirectional moving base and the robot arm. The 2D LiDAR has 3 degrees of freedom by the omnidirectional moving base. We applied a leg detection filter to the lower-equipped 2D LiDAR measurements of HSR to exclude the walls and other objects. We used the same model weights of ProHMR as Sec. V-A. For the quantitative evaluation, the ground truth poses are measured by markerless human motion capture



Fig. 3: Evaluated poses in two pose groups: standing and sitting.

EasyMocap [1]. EasyMocap utilizes multiple calibrated RGB environmental cameras to satisfy enough accuracy to create the human motion dataset ZJU-Mocap [8]. We used six calibrated cameras to utilize EasyMocap.

#### C. Quantitative Results on Real-World Experiments

We evaluated the accuracy of the estimated poses of ten subjects. Eight poses in each of the two pose groups were captured for each subject. Therefore, 160 poses are evaluated in total. HSR estimates the pose with our active measurement and sensor fusion from a constant 0.7-meter distance to the subject, where 3D point cloud sensor measurements frequently drop due to the out-of-range depending on the posture. HSR starts from 8 different positions surrounding the subject with 45 degree intervals. The viewpoint is optimized to be one of eight directions with 45-degree intervals and one of three heights by grid search as described in Sec. IV-C. The subjects are directed to take poses in two groups: standing and sitting, as shown in Fig. 3. The subjects are 163-187 centimeter-tall adults with around 60-110 kilogram weights. The project of this experiment obtained approval from the Research Ethics Review Committee of Toyota Motor Corporation on July 31st, 2023.

We report the mean Euclidean distance error in Tab. II and Tab. III. Unlike previous standard benchmarks such as 3DPW-OC, as shown in Tab. I, we didn't offset the global translation error for a more realistic assumption. JOTR [22], which achieved the best performance among the camerabased methods on 3DPW-OC, results in high Euclidean distance error. This poor performance is because severe truncations as shown in the second row of Fig. 3 cause poorly estimated 2D poses that JOTR heavily depends on during inference. On the other hand, the proposed method achieved the lowest Euclidean distance error averaged on all joints in both pose groups. Our camera active measurement can significantly decrease the estimation error. Sensor fusion of touch sensors can reduce the error of all joints by sensing the whole body relatively freely and complementing

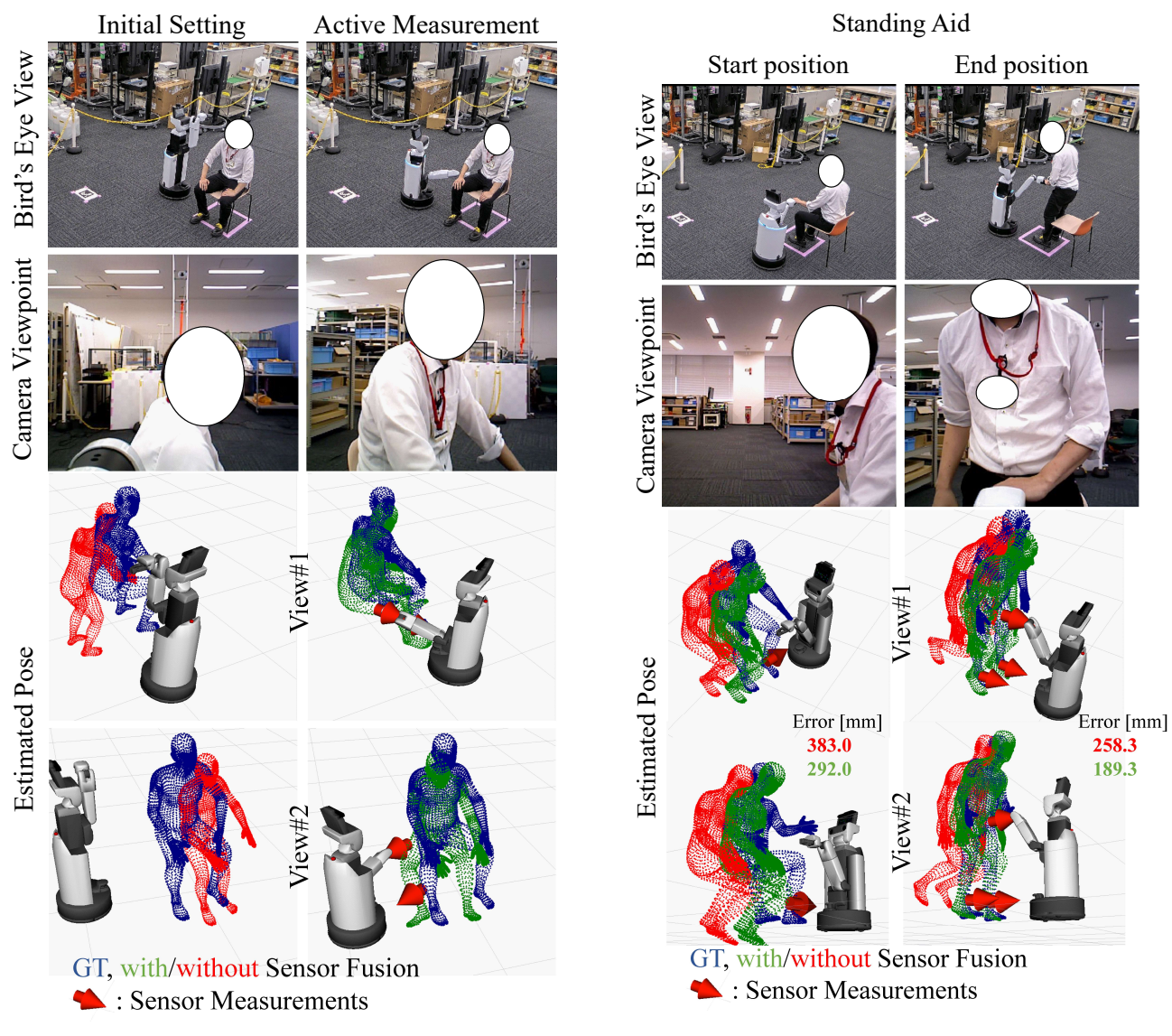


Fig. 4: Visualization of quantitative evaluation.

Fig. 5: Visualization of the standing aid scenario.

limited information from the camera. In contrast, 2D LiDAR mainly improves the estimation of leg poses by sensing the occupation near the floor. 2D LiDAR can reduce the error of ankle joints to half in the standing pose group. The estimated poses are visualized in Fig. 4.

#### D. Estimation Accuracy under Practical Constraints

The quantitative evaluations prove the effectiveness of our method with no restriction on camera and sensor placements in Sec. V-C. However, the practical pHRI scenarios have several restrictions depending on the target task.

**Standing Aid Scenario.** When assistive robots support human bodies or hand something to a person, robot arms must reach certain positions while estimating accurate poses for fall detection. Therefore, the placement of the touch sensor equipped at the end effector is constrained in standing aid scenarios, as shown in the top row of Fig. 5. We mocked this situation and experimented with the standing aid scenario.

The HSR optimizes the camera viewpoint while its end effector follows a specific lifting trajectory. The estimated poses are visualized at the bottom of Fig. 5. The proposed method estimates the poses closer to the ground truth even with the placement constraint on the touch sensor. The

viewpoint is improved from the side low view to the front

high view to cover the larger body while following the target person standing up. The sensor fusion of 2D LiDAR also

improves the leg positions.

Occluded by a Blanket Scenario. Active measurement on camera viewpoints may not be effective in several cases. For example, the target person is sitting under a comforter on a bed or blanket. Assistive robots must estimate accurate poses for posture evaluation to prevent bedsores. Furthermore, wearing loose-fitting clothes such as dresses, hospital patient gowns, and kimonos also affects viewpoint optimization. However, the proposed method can still estimate the accurate

pose thanks to multimodality because touch sensors are

TABLE II: Quantitative results on standing poses.

Base Model	Active Measurement & Sensor Fusion			Euclidean Distance Error [mm]						
	Camera	Touch Sensor	2D LiDAR	Head	Pelvis	R Wrist	L Wrist	R Ankle	L Ankle	All Joints
JOTR [22]				579.1	513.5	532.3	537.3	540.0	548.7	5298
ProHMR [21]				400.4	370.7	437.3	409.1	533.4	547.5	418.1
	$\checkmark$			210.6	224.4	274.0	275.4	428.7	442.5	266.5
	$\checkmark$	$\checkmark$		210.2	201.5	256.6	264.3	387.1	400.8	249.8
	$\checkmark$		$\checkmark$	276.5	215.9	288.2	298.8	210.7	210.5	243.0
	$\checkmark$	$\checkmark$	$\checkmark$	269.1	203.9	275.8	287.6	202.8	215.8	235.9

TABLE III: Quantitative results on sitting poses.

Base Model	Active Measurement & Sensor Fusion			Euclidean Distance Error [mm]						
	Camera	Touch Sensor	2D LiDAR	Head	Pelvis	R Wrist	L Wrist	R Ankle	L Ankle	All Joints
JOTR [22]				543.3	582.3	528.0	586.6	795.3	819.9	584.7
				452.7	514.0	515.2	510.6	791.3	759.5	572.4
ProHMR [21]	✓			206.3	273.9	322.1	298.5	539.1	534.4	322.9
	$\checkmark$	✓		219.3	212.6	293.0	264.1	446.9	449.9	284.2
	$\checkmark$		$\checkmark$	206.1	199.1	267.6	254.2	442.9	415.4	274.9
	✓	✓	$\checkmark$	210.3	192.7	267.1	249.5	419.4	405.8	270.0



Fig. 6: Visualization of the scenario of the target person with a blanket.

robust to these occlusions and reliably obtain the body surface information.

We experimented with a scenario where a blanket occluded the target person. HSR estimates the poses of the target person with a blanket on the person's lower body. The 2D LiDAR measurements were not utilized because the leg detection filter could not detect the leg due to the broad blanket surface. All leg detections around the subjects are filtered out by confidence threshold due to too large diameters of blanket surface for human legs. The estimated poses are visualized in Fig. 6. The proposed method estimates the poses closer to the ground truth by utilizing touch sensor measurement despite poor information from the camera.

#### VI. DISCUSSION

In this section, we discuss the validity of our experimental setting with a single camera and additional sensors.

Multiple Calibrated Environmental cameras may estimate accurate poses as EasyMocap [1] and ZJU-Mocap dataset [8]. However, environmental cameras face serious privacy problems. Usually, no environmental camera is allowed in restrooms because of privacy violations to others despite the need for standing aid of elderly or physically challenged people. Furthermore, environmental cameras are not available outside the buildings. Utilizing only a camera mounted to the standalone robot body is straightforward.

Multiple cameras on multiple robot arms may also estimate accurate poses by triangulation and more visible

area. However, due to cost constraints, robots usually don't equip high DoF arms only for camera observation as Spot of Boston Dynamics, mobile manipulator of Everyday Robots, and Mobile ALOHA [9]. Although we didn't conduct experiments with multiple cameras for the above reason, our method can easily be extended to accept multiple images.

# VII. CONCLUSION

In this paper, we proposed an active measurement and sensor fusion framework for human pose estimation that can estimate accurate human poses in close proximity. Experimental results demonstrated that our method achieved higher accuracy than methods without active measurement or sensor fusion, even with severely truncated camera images.

Our proposed method has several limitations: slow inference and not utilizing temporal information. Our method takes 0.5 seconds to estimate poses due to the optimization in the sensor fusion. We can achieve faster inference by replacing the optimization with regression [27]. In addition to this, we can incorporate temporal information or a previously estimated pose to skip the several processes in our proposed method.

### REFERENCES

- [1] Easymocap make human motion capture easier. Github, 2021.
- [2] Mojtaba Ahangar Arzati and Siamak Arzanpour. Viewpoint selection for dermdrone using deep reinforcement learning. In *IEEE Interna*tional Conference on Control, Automation and Systems, ICCAS, 2021.

- [3] Benjamin Biggs, David Novotný, Sébastien Ehrhardt, Hanbyul Joo, Benjamin Graham, and Andrea Vedaldi. 3d multi-bodies: Fitting sets of plausible 3d human models to ambiguous image data. In Annual Conference on Neural Information Processing Systems, NeurIPS, 2020
- [4] Federica Bogo, Angjoo Kanazawa, Christoph Lassner, Peter V. Gehler, Javier Romero, and Michael J. Black. Keep it SMPL: automatic estimation of 3d human pose and shape from a single image. In European Conference on Computer Vision, ECCV, 2016.
- [5] Zhe Cao, Tomas Simon, Shih-En Wei, and Yaser Sheikh. Realtime multi-person 2d pose estimation using part affinity fields. In IEEE Conference on Computer Vision and Pattern Recognition, CVPR, 2017.
- [6] Kai-Chi Chan, Cheng-Kok Koh, and C. S. George Lee. Selecting best viewpoint for human-pose estimation. In *IEEE International Conference on Robotics and Automation, ICRA*, 2014.
- [7] Hongsuk Choi, Gyeongsik Moon, JoonKyu Park, and Kyoung Mu Lee. Learning to estimate robust 3d human mesh from in-the-wild crowded scenes. In *IEEE/CVF Conference on Computer Vision and Pattern Recognition, CVPR*, 2022.
- [8] Qi Fang, Qing Shuai, Junting Dong, Hujun Bao, and Xiaowei Zhou. Reconstructing 3d human pose by watching humans in the mirror. In IEEE Conference on Computer Vision and Pattern Recognition, CVPR, 2021.
- [9] Zipeng Fu, Tony Z Zhao, and Chelsea Finn. Mobile aloha: Learning bimanual mobile manipulation with low-cost whole-body teleoperation. arXiv preprint arXiv:2401.02117, 2024.
- [10] Yarin Gal and Zoubin Ghahramani. Dropout as a bayesian approximation: Representing model uncertainty in deep learning. In *ICML*, pages 1050–1059, 2016.
- [11] Renshu Gu, Gaoang Wang, and Jenq-Neng Hwang. Exploring severe occlusion: Multi-person 3d pose estimation with gated convolution. In 25th International Conference on Pattern Recognition, ICPR, 2020.
- [12] Yinghao Huang, Manuel Kaufmann, Emre Aksan, Michael J. Black, Otmar Hilliges, and Gerard Pons-Moll. Deep inertial poser: learning to reconstruct human pose from sparse inertial measurements in real time. ACM Trans. Graph., 37(6):185, 2018.
- [13] Ehsan Jahangiri and Alan L. Yuille. Generating multiple diverse hypotheses for human 3d pose consistent with 2d joint detections. In *IEEE International Conference on Computer Vision Workshops*, ICCVW, 2017.
- [14] Haiyong Jiang, Jianfei Cai, and Jianmin Zheng. Skeleton-aware 3d human shape reconstruction from point clouds. In IEEE/CVF International Conference on Computer Vision, ICCV, 2019.
- [15] Angjoo Kanazawa, Michael J. Black, David W. Jacobs, and Jitendra Malik. End-to-end recovery of human shape and pose. In *IEEE Conference on Computer Vision and Pattern Recognition, CVPR*, 2018.
- [16] Alex Kendall and Yarin Gal. What uncertainties do we need in bayesian deep learning for computer vision? *NeurIPS*, 30, 2017.
- [17] Rawal Khirodkar, Shashank Tripathi, and Kris Kitani. Occluded human mesh recovery. In IEEE/CVF Conference on Computer Vision and Pattern Recognition, CVPR, 2022.
- [18] Sena Kiciroglu, Helge Rhodin, Sudipta N. Sinha, Mathieu Salzmann, and Pascal Fua. Activemocap: Optimized viewpoint selection for active human motion capture. In *IEEE/CVF Conference on Computer Vision and Pattern Recognition*, CVPR, 2020.
- [19] Imry Kissos, Lior Fritz, Matan Goldman, Omer Meir, Eduard Oks, and Mark Kliger. Beyond weak perspective for monocular 3d human pose estimation. In European Conference on Computer Vision Workshops, ECCVW, 2020.
- [20] Muhammed Kocabas, Chun-Hao P. Huang, Otmar Hilliges, and Michael J. Black. PARE: part attention regressor for 3d human body estimation. In *IEEE/CVF International Conference on Computer* Vision, ICCV, 2021.
- [21] Nikos Kolotouros, Georgios Pavlakos, Dinesh Jayaraman, and Kostas Daniilidis. Probabilistic modeling for human mesh recovery. In IEEE/CVF International Conference on Computer Vision, ICCV, 2021.
- [22] Jiahao Li, Zongxin Yang, Xiaohan Wang, Jianxin Ma, Chang Zhou, and Yi Yang. JOTR: 3d joint contrastive learning with transformers for occluded human mesh recovery. In *IEEE/CVF International Conference on Computer Vision*, ICCV, 2023.
- [23] Matthew Loper, Naureen Mahmood, Javier Romero, Gerard Pons-Moll, and Michael J. Black. SMPL: a skinned multi-person linear model. ACM Trans. Graph., 34(6):248:1–248:16, 2015.
- [24] Dushyant Mehta, Helge Rhodin, Dan Casas, Pascal Fua, Oleksandr Sotnychenko, Weipeng Xu, and Christian Theobalt. Monocular 3d human pose estimation in the wild using improved CNN supervision. In *International Conference on 3D Vision, 3DV*, 2017.
- [25] Volodymyr Mnih, Koray Kavukcuoglu, David Silver, Alex Graves,

- Ioannis Antonoglou, Daan Wierstra, and Martin A. Riedmiller. Playing atari with deep reinforcement learning. *CoRR*, abs/1312.5602, 2013.
- [26] Gyeongsik Moon and Kyoung Mu Lee. I2l-meshnet: Image-to-lixel prediction network for accurate 3d human pose and mesh estimation from a single RGB image. In European Conference on Computer Vision, ECCV, 2020.
- [27] Takeru Oba and Norimichi Ukita. Data-driven stochastic motion evaluation and optimization with image by spatially-aligned temporal encoding. In *IEEE International Conference on Robotics and Automa*tion, ICRA, 2023.
- [28] Xi Peng, Zhiqiang Tang, Fei Yang, Rogério Schmidt Feris, and Dimitris N. Metaxas. Jointly optimize data augmentation and network training: Adversarial data augmentation in human pose estimation. In IEEE/CVF Conference on Computer Vision and Pattern Recognition, CVPR, 2018.
- [29] Akash Sengupta, Ignas Budvytis, and Roberto Cipolla. Hierarchical kinematic probability distributions for 3d human shape and pose estimation from images in the wild. In *ICCV*, pages 11219–11229, 2021.
- [30] Yu Sun, Qian Bao, Wu Liu, Yili Fu, Michael J. Black, and Tao Mei. Monocular, one-stage, regression of multiple 3d people. In *IEEE/CVF International Conference on Computer Vision*, ICCV, 2021.
- [31] Timo von Marcard, Roberto Henschel, Michael J. Black, Bodo Rosenhahn, and Gerard Pons-Moll. Recovering accurate 3d human pose in the wild using imus and a moving camera. In *European Conference on Computer Vision*, ECCV, 2018.
- [32] Timo von Marcard, Bodo Rosenhahn, Michael J. Black, and Gerard Pons-Moll. Sparse inertial poser: Automatic 3d human pose estimation from sparse imus. *Comput. Graph. Forum*, 36(2):349–360, 2017.
- [33] Bastian Wandt and Bodo Rosenhahn. Repnet: Weakly supervised training of an adversarial reprojection network for 3d human pose estimation. In *IEEE Conference on Computer Vision and Pattern Recognition, CVPR*, 2019.
- [34] Kangkan Wang, Jin Xie, Guofeng Zhang, Lei Liu, and Jian Yang. Sequential 3d human pose and shape estimation from point clouds. In IEEE/CVF Conference on Computer Vision and Pattern Recognition, CVPR, 2020.
- [35] Shih-En Wei, Varun Ramakrishna, Takeo Kanade, and Yaser Sheikh. Convolutional pose machines. In *IEEE Conference on Computer Vision and Pattern Recognition*, CVPR, 2016.
- [36] Fu Xiong, Boshen Zhang, Yang Xiao, Zhiguo Cao, Taidong Yu, Joey Tianyi Zhou, and Junsong Yuan. A2J: anchor-to-joint regression network for 3d articulated pose estimation from a single depth image. In IEEE/CVF International Conference on Computer Vision, ICCV, 2019.
- [37] Yuanlu Xu, Wenguan Wang, Tengyu Liu, Xiaobai Liu, Jianwen Xie, and Song-Chun Zhu. Monocular 3d pose estimation via pose grammar and data augmentation. *IEEE Trans. Pattern Anal. Mach. Intell.*, 44(10):6327–6344, 2022.
- [38] Takashi Yamamoto, Tamaki Nishino, Hideki Kajima, Mitsunori Ohta, and Koichi Ikeda. Human support robot (HSR). In ACM Special Interest Group on Computer Graphics and Interactive Techniques Conference, SIGGRAPH, 2018.
- [39] Takashi Yamamoto, Koji Terada, Akiyoshi Ochiai, Fuminori Saito, Yoshiaki Asahara, and Kazuto Murase. Development of human support robot as the research platform of a domestic mobile manipulator. ROBOMECH journal, 6(1):1–15, 2019.
- [40] Ye Yuan, Umar Iqbal, Pavlo Molchanov, Kris Kitani, and Jan Kautz. GLAMR: global occlusion-aware human mesh recovery with dynamic cameras. In *IEEE/CVF Conference on Computer Vision and Pattern Recognition*, CVPR, 2022.
- [41] Hongwen Zhang, Yating Tian, Xinchi Zhou, Wanli Ouyang, Yebin Liu, Limin Wang, and Zhenan Sun. Pymaf: 3d human pose and shape regression with pyramidal mesh alignment feedback loop. In IEEE/CVF International Conference on Computer Vision, ICCV, 2021.
- [42] Jianfeng Zhang, Xuecheng Nie, and Jiashi Feng. Inference stage optimization for cross-scenario 3d human pose estimation. In Annual Conference on Neural Information Processing Systems, NeurIPS, 2020
- [43] Tianshu Zhang, Buzhen Huang, and Yangang Wang. Object-occluded human shape and pose estimation from a single color image. In IEEE/CVF Conference on Computer Vision and Pattern Recognition, CVPR, 2020.